

# Can single O stars produce non-thermal radio emission?

S. Van Loo<sup>1,2</sup>, M.C. Runacres<sup>1,3</sup> and R. Blomme<sup>1</sup>

<sup>1</sup> Royal Observatory of Belgium, Ringlaan 3, B-1180 Brussel, Belgium

<sup>2</sup> School of Physics and Astronomy, University of Leeds, Leeds LS2 9JT, UK

<sup>3</sup> Vrije Universiteit Brussel, Pleinlaan 2, B-1050 Brussel, Belgium

Received / Accepted

## ABSTRACT

We present a model for the non-thermal radio emission from presumably single O stars, in terms of synchrotron emission from relativistic electrons accelerated in wind-embedded shocks. These shocks are associated with an unstable, chaotic wind. The main improvement with respect to earlier models is the inclusion of the radial dependence of the shock velocity jump and compression ratio, based on one-dimensional time-dependent hydrodynamical simulations. The decrease of the velocity jump and the compression ratio as a function of radius produces a rapidly decreasing synchrotron emissivity. This effectively prohibits the models from reproducing the spectral shape of the observed non-thermal radio emission. We investigate a number of “escape routes” by which the hydrodynamical predictions might be reconciled with the radio observations. We find that the observed spectral shape can be reproduced by a slower decline of the compression ratio and the velocity jump, by the re-acceleration of electrons in many shocks or by adopting a lower mass-loss rate. However, none of these escape routes are physically plausible. In particular, re-acceleration by feeding an electron distribution through a number of shocks, is in contradiction with current hydrodynamical simulations. These hydrodynamical simulations have their limitations, most notably the use of one-dimensionality. At present, it is not feasible to perform two-dimensional simulations of the wind out to the distances required for synchrotron-emission models. Based on the current hydrodynamic models, we suspect that the observed non-thermal radio emission from O stars cannot be explained by wind-embedded shocks associated with the instability of the line-driving mechanism. The most likely alternative mechanism is synchrotron emission from colliding winds. That would imply that all O stars with non-thermal radio emission should be members of binary or multiple systems.

**Key words.** stars: early-type – stars: winds, outflows – radiation mechanisms: non-thermal – hydrodynamics – instabilities – binaries: general

## 1. Introduction

Hot stars are sources of both thermal and non-thermal radio emission. The *thermal* radiation is free-free emission from thermal electrons in the ionised stellar wind. As all hot stars have winds, they are all expected to have thermal emission, although it is intrinsically faint and can only be detected for the brightest and closest stars. A significant fraction of hot stars also emits *non-thermal* radiation, which is generally attributed to synchrotron emission from relativistic electrons.

Wright & Barlow (1975) developed an elegant formalism for the thermal radio emission from hot stars. Assuming a uniform, isothermal, spherically symmetric outflow, they showed that the expected flux is of the form  $F_\nu \propto \nu^\alpha$ , where the spectral index  $\alpha = +0.6$ . The same formalism allows a star’s mass-loss rate to be derived from its thermal radio flux.

Non-thermal emission from hot stars is generally much stronger than thermal emission, and strongly variable (the O5 supergiant Cyg OB2 No. 9, for instance, was observed to vary

by a factor of ten at 6 cm by Bieging et al. 1989). It also has a very different spectral shape, with a negative spectral index, i.e. a flux that decreases as a function of frequency. Such a spectrum is characteristic of synchrotron emission from relativistic electrons gyrating in a magnetic field. Electrons can attain relativistic speeds through first order Fermi acceleration in shocks (Bell 1978, Drury 1983). Although shock-acceleration has been most frequently used to explain synchrotron emission from hot stars, other mechanisms such as magnetic reconnection are also capable of accelerating particles to relativistic speeds (e.g. Litvinenko 2003).

A fundamental question regarding non-thermal radio emission from O stars is its correlation with binarity. If the non-thermal emitter is a member of a binary system, the shocks needed to accelerate the electrons can be provided by colliding stellar winds. This is the case for Wolf-Rayet stars, where the correlation between non-thermal radio emission and binarity is firmly established, and binarity appears to be a prerequisite for non-thermal emission (Dougherty & Williams 2000). The situation is less clear for O stars. Of the 16 currently known non-

**Table 1.** Binary status of non-thermal radio emitting O stars. The list is compiled from Biegging et al. (1989, a), Persi et al. (1985, b), Leitherer et al. (1995, c), Benaglia et al. (2001, d), Setia Gunawan et al. (2003, e), Benaglia & Koribalski (2004, f) and Drake (1990, g).

Name	Spectral Type	Binary Status	NT Ref.
HD 93129A	O2 If + ?	BIN <sup>1</sup>	f
HD 93250	O3 V((f))	-	c
9 Sgr	O4 V	-	a
CD-47°4551	O5 If	-	d
Cyg OB2 No. 9	O5 If	-	a
HD 150136	O5 III <sub>n</sub> (f) + ?	BIN <sup>2</sup>	d
HD 168112	O5 III	-	a
HD 15558	O5 III + ?	BIN <sup>3</sup>	a
Cyg OB2 No. 8A	O6 + O5.5	BIN <sup>4</sup>	a
Cyg OB2 No. 5	O6 f + O7 f	BIN <sup>5</sup>	b
HD 124314	O6 V(n)((f)) + ?	BIN <sup>6</sup>	d
Cyg OB2-335	O7 V	-	e
15 Mon	O7 Ve	BIN <sup>8</sup>	g
HD 167971	O7.5 Vf + O	BIN <sup>7</sup>	a
δ Ori A	O9.5 II + ?	BIN <sup>9</sup>	g
σ Ori AB	O9.5 V + ?	BIN <sup>10</sup>	g

<sup>1</sup> Walborn (2002); <sup>2</sup> Garmany et al. (1980); <sup>3</sup> Garmany & Massey (1981); <sup>4</sup> De Becker et al. (2004); <sup>5</sup> Torres-Dodgen et al. (1991); <sup>6</sup> Gies (1987); <sup>7</sup> Leitherer et al. (1987); <sup>8</sup> Gies et al. (1993); <sup>9</sup> Harvey et al. (1987); <sup>10</sup> Bolton (1974)

thermal radio emitting O stars, only 10 are confirmed binaries (Table 1).

A priori, there is no need for non-thermal emitters to be binaries. The driving mechanism of hot-star winds is known to be subject to a line-deshadowing instability (Owocki & Rybicki 1984, Feldmeier 2001). Time-dependent hydrodynamical simulations including the line-deshadowing instability (e.g. Runacres & Owocki 2002), show that it produces a wealth of shocks that in principle are capable of accelerating electrons to high speeds. We refer to these shocks as wind-embedded shocks. Non-thermal radio emission from hot stars was first interpreted as synchrotron emission from electrons accelerated in such wind-embedded shocks by White (1985). Substantial improvements of this original idea were made by Chen (1992) and Chen & White (1994).

This is the third in a series of papers investigating the non-thermal radio emission from single stars. The general aim is to determine the properties that wind-embedded shock models must have to reproduce the observed non-thermal radio emission. By this means, we are also able to shed some light on the fundamental question of binarity, as it will become clear to what extent the wind-embedded shock model is able to explain the observations. Such an indirect approach is necessary because it is difficult, in general, to confirm observationally that a star is single. A failure of the wind-embedded shock model to explain the observations would strongly suggest that colliding winds are required to produce non-thermal radio emission.

In Van Loo et al. (2004, hereafter Paper I), we introduced a simple parametrised model. The number distribution of synchrotron-emitting electrons was given by a power law, both as a function of momentum and distance. The emission region was assumed to extend *continuously* out to an outer radius  $R_{\max}$ . This assumption is open to criticism, because cooling mechanisms such as inverse Compton scattering can limit the emission to potentially thin layers behind the shocks (Chen 1992). This effect was included in Van Loo et al. (2005, hereafter Paper II). In that paper we found that the emitting layers can indeed be quite narrow and are also few in number, because the strongest shocks tend to dominate the emission. In the present paper, we further extend the model to take into account the fact that shocks gradually weaken as they move out with the flow. Specifically, we use results of time-dependent hydrodynamical simulations as input to our synchrotron-emission models.

The comparison of synchrotron spectra with hydrodynamical simulations of instability-generated structure has the additional advantage of providing supplementary observational input for such simulations. Although the theoretical argument for the line-deshadowing instability is extremely strong (Owocki 1991), and the instability-generated structure is still the best explanation for, e.g., soft X-ray emission, black troughs, and clumping inferred from density-squared diagnostics (e.g. Owocki 1991), the small-scale inhomogeneities it generates are not easy to detect. Therefore, any additional observational information about such structure would be most welcome.

The remainder of this paper is organised as follows. In Sect. 2 we introduce the model. In Sect. 3 we conclude that it fails to explain the Cyg OB2 No. 9 observations. We explore various “escape routes” in Sect. 4. Conclusions are given in Sect. 5.

## 2. The model

### 2.1. Layered emission

As the present model is based on the one from Paper II, we briefly review the properties of this latter model. The synchrotron emission is produced by electrons accelerated in wind-embedded shocks, produced by the line-deshadowing instability in a single star wind. The acceleration is not calculated *ab initio*, but a power law is assumed for the momentum distribution of electrons.

In principle, the pressure from the relativistic particles can influence the structure of the shocks, and can even lead to their destruction (Drury 1983). Incorporating this influence in time-dependent hydrodynamical simulations is beyond the scope of the present work. We therefore neglect the effect of relativistic particles on the hydrodynamics (this is referred to as the “test-particle approach”). The result of incorporating this influence in time-dependent hydrodynamical simulations would be to weaken the shocks, thereby making it more difficult to produce the extended regions of non-thermal emission needed to explain the observations. As we shall find, it is already difficult to produce the observed emission based on present shock strengths (Sect. 2.2), so our conclusions will be all the more

valid if the feedback of relativistic particles on the hydrodynamics is included.

We adopt the magnetic field expression of Weber & Davis (1967). This means that, at large distances from the star, the magnetic field is almost perpendicular to the shock normal. Jokipii (1987) showed that this configuration (i.e. quasi-perpendicular shocks) is the most efficient for particle acceleration. Details are given in Van Loo (2005).

The electrons are subject to a number of cooling mechanisms, most notably inverse Compton scattering and adiabatic expansion. Cooling has an important effect both at the shock front, and downstream. At the shock front, the maximum attainable energy is set by the balance between acceleration and cooling, imposing a high-momentum cut-off on the distribution. Downstream from the shock, the acceleration ceases and cooling rapidly removes the energy of relativistic electrons. The emission is then expected to come not from a continuous volume, but from a (possibly thin) layer behind each shock. Cooling also modifies the shape of the momentum distribution close to the cut-off. Away from the cut-off it retains its power-law shape.

In Paper II, we also showed that the strongest shocks dominate the emission. This means that the number of synchrotron emission layers that contribute substantially to the observed emission is small. It is therefore natural to consider first the case of a single shock. A single-shock model is characterised by four free parameters: the position  $R_S$  of the shock, its velocity jump  $\Delta u$  and its compression ratio  $\chi$ , and the surface magnetic field  $B_*$ . The fluxes include a small but significant thermal contribution (25% of the total flux at 2 cm). For a complete discussion of the model, we refer to Paper II.

To describe the distribution behind the shock front, we need to know where the electrons were accelerated and how they are cooled. The relativistic electrons move away from the shock front with the gas. In terms of the velocity jump  $\Delta u$  and the compression ratio  $\chi$ , the post-shock speed in the frame of the shock can be expressed as

$$u_2 = \frac{\Delta u}{\chi - 1}, \quad (1)$$

which follows directly from the Rankine-Hugoniot relations. As the gas flows a distance  $\Delta R_S$  away from the shock at a speed  $u_2$ , the shock has travelled a much larger distance  $\approx \Delta R_S v_\infty / u_2$ , where  $v_\infty$  is the terminal speed. As  $v_\infty / u_2 \sim 100$ , the electron distribution in a fairly narrow layer behind an outer-wind shock reflects wind conditions over a wide range in distance. The outer electrons of a typical synchrotron-emitting layer ( $4 R_*$  wide, behind a shock at  $500 R_*$ ), will have been accelerated at a distance  $\sim 100 R_*$  from the central star. Of course, they are subjected to severe cooling during the time-interval needed to reach the outer wind.

In Paper II, we assumed a constant shock velocity jump and compression ratio, mainly to keep the number of free parameters in the model as small as possible. However, hydrodynamical simulations show that both the shock velocity jump and the compression ratio decline with radius (see Fig. 1). The shock velocity jump appears as a strong scaling factor in this model,

with the flux proportional to  $\Delta u^3$ . The dependence of the synchrotron flux on the compression ratio  $\chi$  is somewhat more complicated, but is also important (Van Loo 2005). Generally, the flux increases rapidly with  $\chi$ . In view of the wide range in radius reflected by the electron distribution, one can therefore expect that introducing the radial decline of the velocity jump and the compression ratio has important consequences for the models.

Due to the free-free opacity of the dense stellar wind, any radio emission (thermal or non-thermal) that is emitted too close to the star will be absorbed. Roughly speaking, the emergent radio flux originates beyond the radius of unit free-free optical depth. This radius can be viewed as a kind of ‘‘radio photosphere’’ of the stellar wind. Due to the wavelength-squared dependence of the free-free opacity, the size of the radio photosphere increases with wavelength. For example, in the well-studied non-thermal radio emitting O star Cyg OB2 No. 9, the radio photosphere is  $90 R_*$  at 2 cm (15 GHz) and  $195 R_*$  at 6 cm (5 GHz). The emergent flux of a non-thermal emitter is determined by the tight interplay between non-thermal emission and thermal absorption. This is what gives the models their great diagnostic value. A more detailed discussion of the radio formation region is given in Paper I.

## 2.2. Hydrodynamical input

Since the pioneering models of Owocki et al. (1988), many hydrodynamical simulations of hot-star winds have included the line-deshadowing instability (e.g. Feldmeier 1995, Dessart & Owocki 2002, Runacres & Owocki 2002). These simulations show that within a few stellar radii of the surface, the flow becomes highly structured, with gas concentrated in dense clumps, and pervaded by strong shocks. These simulations are restricted to distances smaller than  $100 R_*$ , which is not far enough to provide input for synchrotron-emission models. For simulations extending out to large radii, Runacres & Owocki (2005) introduced a periodic-box formalism for the outer evolution of structure in hot-star winds, which enabled them to follow structure out to distances of more than  $1000 R_*$ .

In Fig. 1 we show the velocity jump and compression ratio of a typical strong shock in a periodic-box model as it moves out with the gas. The shock velocity jump steadily decreases from  $\gtrsim 100 \text{ km s}^{-1}$  at  $100 R_*$  to  $\approx 55 \text{ km s}^{-1}$  at  $250 R_*$  and further to  $\approx 20 \text{ km s}^{-1}$  beyond  $500 R_*$ . The compression ratio rises from  $\approx 2.6$  at  $100 R_*$  to  $3.3$  at  $250 R_*$ , and then decreases to values  $\approx 2.2$  beyond  $500 R_*$ . The compression ratio increases between  $100$  and  $200 R_*$  because the strong forward shock that we follow overtakes a few weak forward shocks and merges with them.

As it takes some time to cool relativistic electrons below radio-emitting energies, the inner-wind accelerated electrons can contribute significantly to the radio emission. Furthermore, since the emissivity rapidly declines with radius due to the decreasing shock velocity jump and compression ratio, the emergent flux is weighted in favour of electrons accelerated in the inner wind, and the radial dependence of the velocity jump and the compression ratio must be included in the model. For the

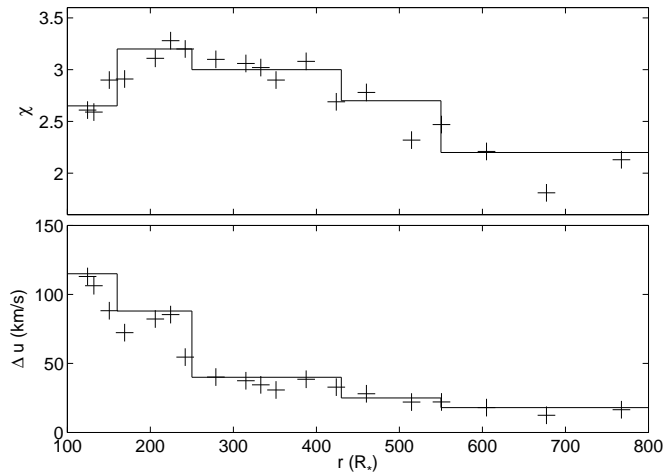


**Fig. 1.** Compression ratio (plus signs, upper panel) and velocity jump (plus signs, lower panel) of a typical shock in the periodic-box model of Runacres & Owocki (2005), as a function of radius. The solid lines represent the step function approximations used in the code.

sake of simplicity, we approximate the radial dependence of  $\Delta u$  and  $\chi$  by step functions of the form shown in Fig. 1.

### 3. Results

#### 3.1. Single shock

In a single-shock model, explicitly taking into account the radial dependence of  $\Delta u$  and  $\chi$  has an important effect on the emergent flux. In Paper II we showed that a single shock located at  $\sim 600 R_*$  can explain the observed non-thermal emission of Cyg OB2 No. 9, albeit with a much larger velocity jump ( $290 \text{ km s}^{-1}$ ) than predicted by hydrodynamical simulations. From Fig. 1 we derive that a typical shock at that distance has a compression ratio  $\chi = 2.2$  and a velocity jump  $\Delta u = 18 \text{ km s}^{-1}$ . In Paper II we assumed that the shock strength is the same everywhere in the wind, whereas the hydrodynamical simulations predict a weakening of the shock. It is to be expected, for a weak outer-wind shock, that its past history as a stronger inner-wind shock affects the energy distribution of the accelerated electrons behind it.

In Fig. 2 we compare the pure synchrotron flux (without the thermal contribution) generated by such a single shock assuming a constant shock strength throughout the wind (dashed line), and the flux emitted by the same shock when its history is taken into account (solid line). This last model produces significantly more emission (by a factor of  $\sim 200$ ). This is because, when the shock was closer to the star and consequently stronger, it produced a population of electrons that are still sufficiently energetic, in spite of strong inverse-Compton cooling, to produce synchrotron emission.

When the history of the shock is taken into account, a single shock can still explain the observed non-thermal spectrum of Cyg OB2 No. 9. To fit the observed flux, we need to adjust the

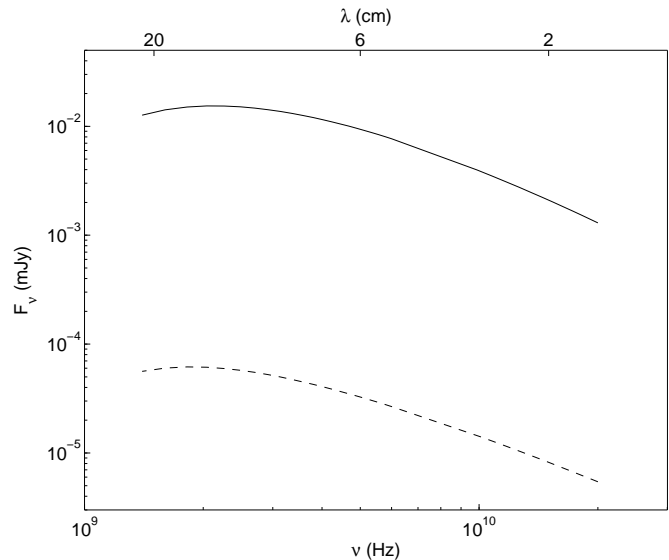


**Fig. 2.** Pure synchrotron flux for a single-shock model with declining  $\Delta u$  and  $\chi$  given by the step functions in Fig. 1 (solid line), compared to a model with constant shock strength  $\chi = 2.2$  and  $\Delta u = 18 \text{ km s}^{-1}$  (dashed line), i.e. a model where the history of the shock has not been taken into account. The shock is located at  $R_S = 600 R_*$ . The surface magnetic field is  $B_* = 200 \text{ G}$ . Stellar and wind parameters are as in Paper II.

magnitude of the shock velocity jump. We do this by defining the velocity jump at radius  $r$  as

$$\Delta u(r) = \Delta u_{\text{max}} f(r), \quad (2)$$

where  $f(r)$  is the velocity jump from Fig. 1, divided by its highest value (i.e.  $f(r) \leq 1$ ), and  $\Delta u_{\text{max}}$  is a scaling factor that sets the magnitude of the velocity jump.

In Fig. 3 we show a single-shock model that fits the observed spectrum. For simplicity, the compression ratio  $\chi$  is taken to be 4 at all radii. The value of  $\Delta u_{\text{max}}$  is  $1050 \text{ km s}^{-1}$ , corresponding to a local velocity jump at  $R_S = 602 R_*$  of  $164 \text{ km s}^{-1}$ . This is lower than the value determined in Paper II (due to the significant amount of inner wind accelerated electrons in the emission layer) but still an order of magnitude higher than predicted by hydrodynamical simulations. With a decreasing  $\chi$ , the value obtained for  $\Delta u$  would be even higher. The only way to fit the observations with smaller velocity jumps is to consider multiple shocks.

#### 3.2. Multiple shocks

##### 3.2.1. Constant $\chi$ and $\Delta u$

The synchrotron emission in our model is proportional to the third power of the shock velocity jump (Paper II). This allows us to estimate the flux of a multiple-shock model with a constant compression ratio and velocity jump from a single-shock model. The condition for a collection of  $N$  identical shocks with velocity jump  $\Delta u$ , distributed throughout the wind, to pro-



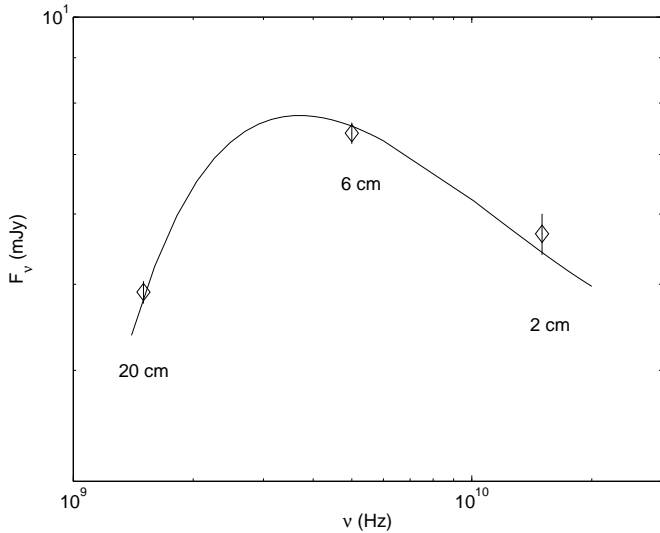


**Fig. 3.** A single-shock model (solid line) that fits the observations (diamonds) of Cyg OB2 No. 9. The vertical stripes are the error bars. The shock velocity jump is  $\Delta u(r) = \Delta u_{\max} f(r)$ , as defined in Eq. (2). The fit parameters are  $\Delta u_{\max} = 1050 \text{ km s}^{-1}$ ,  $R_S = 602 R_*$ ,  $\chi = 4$  and  $B_* = 200 \text{ G}$ .

duce the same flux as a single shock with velocity jump  $\Delta u_{\text{single}}$  is simply expressed as

$$N\Delta u^3 = \Delta u_{\text{single}}^3. \quad (3)$$

This offers a way of lowering the velocity jump needed to explain the observations: one just adds shocks until the velocity jump is in the range of the hydrodynamical predictions. In Paper II, we fitted the observations by a single shock with  $\Delta u_{\text{single}} = 290 \text{ km s}^{-1}$ . Using the above equation we estimated that 200 shocks with  $\Delta u = 50 \text{ km s}^{-1}$  should produce the same flux.

When the shock velocity jump and/or compression ratio decrease as a function of radius, as predicted by hydrodynamical simulations, Eq. (3) can no longer be applied. In that case, we find that our model cannot reproduce the observations (Sect. 3.2.2). To understand why this is so, it is useful to consider first the *cumulative* flux for a model with a *constant* shock velocity jump and compression ratio. (The cumulative flux at a position  $r$  in the wind is defined as the emergent flux due to all the shocks between the stellar surface and  $r$ .) In Fig. 4 we show the cumulative fluxes at different radio wavelengths for an equidistant distribution of shocks, with a shock at every  $12 R_*$  (The influence of the adopted shock spacing is discussed in Sect. 4.1). All shocks have  $\chi = 3.7$  and  $\Delta u = 71 \text{ km s}^{-1}$ . The surface magnetic field is  $B_* = 200 \text{ G}$ . Only the synchrotron flux is shown. The “observed” synchrotron flux is obtained by subtracting the theoretical thermal flux (using the Wright & Barlow formalism) from the observed radio flux. The cumulative synchrotron flux at 2 cm (solid line) is zero for distances below  $\sim 50 R_*$ , where all synchrotron emission is absorbed by the free-free opacity of the wind, and then rises sharply. The flux at 6 cm (dashed) begins to rise further out, due to the larger free-free optical depth. For the same reason, the 20 cm begins to rise even later.

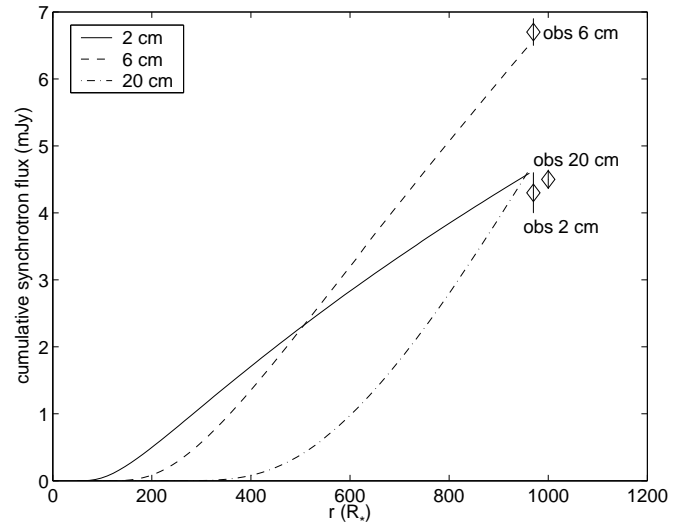


**Fig. 4.** Cumulative fluxes for a model with constant compression ratio and velocity jump, at 2 cm (solid line), 6 cm (dashed) and 20 cm (dashed-dotted). The diamonds are the observed synchrotron fluxes and also the error bar on the observations is given. The model parameters are  $\Delta u = 71 \text{ km s}^{-1}$ ,  $\chi = 3.7$  and  $B_* = 200 \text{ G}$  ( $\Delta u$  and  $\chi$  are constant in the wind). A shock is present every  $12 R_*$ .

The cumulative flux increases more steeply at larger wavelengths. The reason is twofold. First, there is the intrinsic spectrum of synchrotron emission: the flux at larger wavelengths is produced by less energetic electrons, of which there are more by virtue of the shape of the momentum distribution. Second, inverse-Compton cooling is less severe at larger wavelengths, so that the synchrotron-emitting layer is wider.

### 3.2.2. Declining $\chi$ and $\Delta u$

Let us now see what happens when the shock velocity jump and compression ratio decrease as a function of radius, as predicted by hydrodynamical simulations. We can no longer use Eq. (3) to determine how many shocks are needed, but plotting the cumulative flux allows us to judge when we have a good fit to the observations, without requiring the number of shocks to be pre-specified.

In Fig. 5 we show the cumulative flux for a model that is similar to the model shown in Fig. 4, except for the decreasing shock strength. The compression ratio of the shocks is given by Fig. 1 (top panel). The velocity jump is given by the lower panel of the same figure, but a scaling factor  $\Delta u_{\max}$  is introduced, as in Sect. 3.1, to fit the observed flux at 6 cm. In the model shown,  $\Delta u_{\max} = 194 \text{ km s}^{-1}$ , which represents a 70% increase with respect to the hydrodynamical predictions. The cumulative fluxes are zero below the radio photosphere, and then rise steeply. Contrary to the model with constant velocity jump and compression ratio, there is no discernible difference in the rate of increase of the fluxes at 2 and 6 cm. If the shock strength were constant, the 6 cm flux would rise faster than the 2 cm flux (see Sect. 3.2.1). This is now compensated by the fact

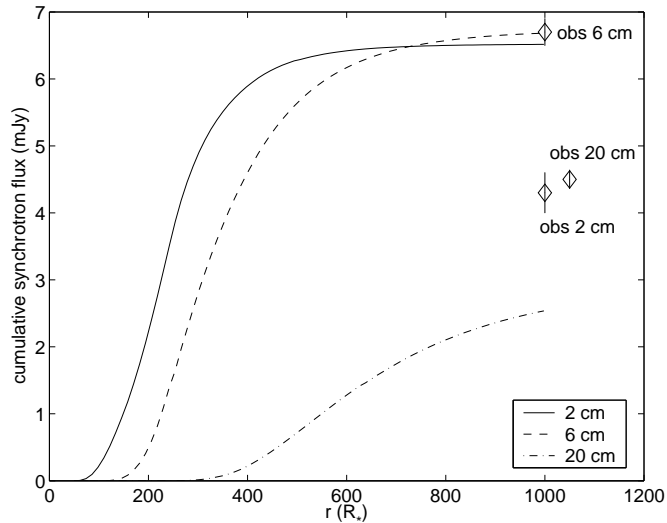


**Fig. 5.** Cumulative fluxes for a model with decreasing compression ratio and velocity jump, at 2 cm (solid line), 6 cm (dashed) and 20 cm (dash-dotted). The diamonds are the observed synchrotron fluxes and also the error bar on the observations is given. The model parameters are  $B_* = 200$  G,  $\Delta u_{\max} = 194$  km s $^{-1}$  and  $\chi$  is taken from Fig. 1. A shock is present every  $12 R_*$ .

that the 2 cm flux is formed at smaller radii, where the shocks are stronger.

Both the 2 and 6 cm fluxes level off at large radii, because the compression ratio and velocity jump become so small that the emitted synchrotron radiation is negligible. The fluxes at 2 and 6 cm reach approximately the same asymptotic value, resulting in a flat synchrotron spectrum. After adding the thermal contribution, the emergent spectrum has a positive slope, contrary to observations. At 20 cm, the model significantly underestimates the observation. Extending the model to larger radii would increase the 20 cm flux somewhat, but would have no effect on the 2 and 6 cm flux.

In summary, we find that a model where the velocity jump and compression ratio are taken from hydrodynamical simulations does not reproduce the observed radio spectrum, because the strong shocks close to the star contribute more to the flux at shorter wavelengths (where the free-free opacity is smaller) than at longer wavelengths. Any model where the emissivity is a strongly decreasing function of radius will therefore have a tendency toward a positive spectral index. Conversely, to reproduce the observed negative spectral index, any model should have an emissivity that is a weakly decreasing function of radius.

## 4. Discussion

The hydrodynamical simulations from which we take the shock velocity jump and compression ratio are subject to considerable uncertainty. Foremost, they are performed in one dimension, whereas the stellar wind is expected to contain a fair amount of lateral structure (e.g. due to Rayleigh-Taylor instabilities, see Dessart & Owocki 2003). Moreover, no attempt has been

made to model a particular star. The results of these simulations should therefore not be taken at face value. To further quantify the discrepancy between the hydrodynamical predictions and the radio observations, let us see by which modifications the two may be reconciled or, in other words, which “escape routes” may lead us away from the discrepancy, and whether any of these escape routes is physically plausible.

### 4.1. Shock spacing and outer boundary of the synchrotron-emitting region

In Sect. 3 we adopted a shock spacing of  $12 R_*$ . This value is somewhat arbitrary but is based on the spacing found in hydrodynamical simulations, and on the fact that only the strongest shocks will contribute substantially to the synchrotron emission. Reducing the spacing from  $12 R_*$  to  $4 R_*$ , which is about the smallest distance between two adjacent outer wind shocks in the hydrodynamical simulations, does not change the slope of the emergent synchrotron spectrum. The only effect of the closer spacing is a lower value of  $\Delta u_{\max}$ , due to the larger number of shocks in the wind.

To produce the observed negative spectral index, the radial decrease of the synchrotron emission should be weak. Such a slow decrease can be obtained by a closer shock spacing in the outer wind than in the inner wind (to counteract the decrease of the shock strength). Physically this corresponds to a slowing down of the shocks as they move out with the wind. Such a slowing down can indeed be expected from momentum conservation. However, the associated change in velocity is minimal. Both the shell and the material it sweeps up are moving at roughly the terminal speed, with velocity differences of the order of a few times the sound speed. We find that, to reproduce the observed spectral index, the spacing of the shocks in the 20 cm formation region should be less than half of that in the 2 cm formation region. This corresponds to a decrease in shock speed (measured in the stellar rest frame) of a factor of two or more, which is not predicted either by detailed hydrodynamical simulations or by the momentum conservation argument above.

The adopted outer boundary of the synchrotron-emitting region could in principle influence the spectral index predicted by the model. However, the fact that the cumulative flux in Fig. 5 levels off at large radii shows that the spectral shape cannot be changed by extending the synchrotron-emitting region to larger radii (as the contribution at large radii becomes negligible).

We conclude that our model cannot be made to produce a negative spectral index by increasing the number of shocks in the wind, either by changing the shock spacing or by adopting a larger outer boundary of the synchrotron-emitting region.

### 4.2. Rate of decline of $\chi$ and $\Delta u$

To reproduce the observed spectra, any model should have an emissivity that does not decline too rapidly as a function of radius. As the emissivity is directly related to the compression ratio and velocity jump of the shocks producing the emission, making these properties a weaker function of radius is a nat-

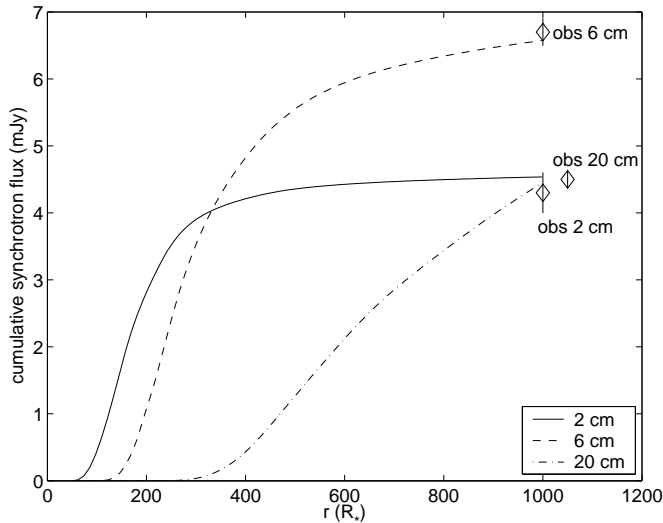


**Fig. 6.** Cumulative fluxes for a model with a “flattened”  $\Delta u(r)$ , at 2 cm (solid line), 6 cm (dashed) and 20 cm (dash-dotted). The diamonds are the observed synchrotron fluxes and also the error bar on the observations is given. The ratio between the maximum and minimum  $\Delta u$  is 3. The other parameters are  $\Delta u_{\max} = 835 \text{ km s}^{-1}$ ,  $\chi = 2$  and  $B_* = 200 \text{ G}$ . A shock is present every  $12 R_*$ .

ural way of obtaining a more slowly declining emissivity. As it is difficult to disentangle the effects of a declining velocity jump and a declining compression ratio, we adopt a constant compression ratio and see how weak a function of radius the velocity jump should be to produce a negative spectral index. Therefore, we make  $\Delta u(r)$  a weaker function of  $r$ , by replacing  $f(r)$  in Eq. (2) with  $\tilde{f}(r)$ , defined as

$$\tilde{f}(r) = 1 - \epsilon [1 - f(r)] \quad 0 < \epsilon < 1 \quad (4)$$

where  $\epsilon = 1$  corresponds to the original  $f(r)$  and  $\epsilon = 0$  to a constant velocity jump. In Fig. 6 we show the cumulative flux for a model where  $\Delta u(r)$  has been “flattened” in this manner and a constant compression ratio  $\chi = 2$ . The ratio between the maximum and minimum values of  $\Delta u$  is 3 (corresponding to  $\epsilon = 0.79$ ), as opposed to 6.4 in Fig. 1. This model explains the observations at all wavelengths, although the required  $\Delta u_{\max}$  is much higher than the hydrodynamical predictions. The observations can also be reproduced with a higher compression ratio  $\chi = 3$  and an even flatter  $\Delta u(r)$ , with a ratio of 1.5 between its maximum and minimum.

In these models, we assumed a constant compression ratio, whereas the hydrodynamical simulations predict a decline (Fig. 1). With a declining compression ratio,  $\Delta u(r)$  must be even flatter.

Indeed, we find that, with  $\chi(r)$  as defined in Fig. 1,  $\Delta u$  must be constant to fit the observations. If  $\chi(r)$  is flattened in the same way as was done above for  $\Delta u(r)$  (Eq. (4)), a fit can be obtained if the ratio between maximum and minimum is 1.3 or less for both  $\Delta u$  and  $\chi$ .

The upshot of the above is that the radio spectrum of Cyg OB2 No. 9 can only be explained with our model with

a modest ( $\leq 30\%$ ) decrease of the velocity jump and compression ratio. The range in radius contributing to the emergent flux at 2, 6 and 20 cm is  $\sim 30 - 1000 R_*$ . Although not absolutely impossible, it is unlikely that shocks would have such a small decrease in velocity jump and compression ratio over such a large distance.

### 4.3. Re-acceleration

Our results show that it is difficult for a wind-embedded shock model to reproduce an observed non-thermal radio spectrum, if the radial decline of the shock strength is in agreement with hydrodynamical predictions. This may seem at odds with some previous models that successfully reproduce the observed non-thermal spectra. The most advanced of these models is given in Chen (1992) and Chen & White (1994). Their model can successfully reproduce the observed non-thermal spectrum of both 9 Sgr and Cyg OB2 No. 9. It includes adiabatic and inverse-Compton cooling. As a result, electrons cannot travel very far from the acceleration site, and the electrons have to be accelerated *in situ* in the radio-emitting region. The emission is then also confined to layers behind the shocks. In that respect, the Chen & White (1994) model is very similar to the model presented in the present paper.

The fundamental difference between Chen & White and the present model is re-acceleration of electrons. If a fluid element goes through a number of successive shocks as it moves outward, then relativistic electrons in the outer wind will, on average, have passed through more shocks than inner-wind electrons. Consequently, these outer-wind electrons are more energetic than they would have been at the same position in the wind, had they passed through only one shock. Therefore, re-acceleration substantially slows down the outward decrease of the synchrotron emissivity and is expected to facilitate a negative spectral index. Indeed, with a simplified model of re-acceleration, where we artificially slow down the radial decrease of the relativistic electron density, we easily reproduce the observations.

Whether or not re-acceleration occurs depends on the adopted hydrodynamical model. In Chen & White (1994), the hydrodynamical model is from Lucy (1982), supplemented with a snowplough model to describe structure in the outer wind (Chen 1992). In Lucy (1982), all shocks are forward shocks. As was pointed out by White (White & Chen 1994, discussion), a fluid element in the Lucy model is accelerated to the terminal speed only in the shock jumps. Therefore, any given fluid element goes through a large number of shocks. Relativistic electrons are then accelerated at one shock front, cool as they travel downstream to the next shock, and are re-accelerated there. A population of new, freshly accelerated relativistic electrons is also created at each shock.

Lucy’s model is entirely phenomenological, however. When the line-deshadowing instability is introduced in a model that solves the time-dependent equations of hydrodynamics, the physical picture of wind structure is quite different. The fundamental consequence of the instability is the omnipresence of strong rarefaction waves of fast, rarefied gas. These rarefac-

tions are terminated by a reverse shock (much as when gas runs into a solid wall), forming the inner boundary of a dense shell. As this dense shell is impacted by faster shells, it develops a forward shock on the outside. The result is that shocks occur in pairs at either side of a dense shell. Gas is fed through the shocks into the shell and then remains trapped there. A fluid element therefore only encounters a single shock, making re-acceleration impossible.

The simulations on which the above analysis is based are one-dimensional. In a three-dimensional situation the trapping of the gas is less absolute, as gas can in principle escape sideways from a shell fragment or blob and encounter another shock. It is hard to make a quantitative estimate of the importance of such an effect. As the radiative driving and the associated instability are strongest in the radial direction, one can expect the azimuthal velocity to be relatively small, even though instabilities such as Rayleigh-Taylor are expected to disrupt the lateral coherence of the structure. One situation where the azimuthal velocity could become more important is the case of rarefied gas flowing around a dense blob. However, this gas has a low density and should therefore not contribute much to the emission. It therefore seems likely that most of the dense gas will see few shocks, which impairs the main mechanism by which Chen & White (1994) were able to produce a negative spectral index.

#### 4.4. Smaller radio photosphere

The main impediment for a strongly decreasing synchrotron emissivity to produce a negative spectral index is the difference in the radio photosphere at 2 and 6 cm, which causes the 2 cm flux to benefit from strong emission that is inaccessible to the 6 cm flux. This difference in radio photosphere increases with density, and hence with the mass-loss rate. It can therefore be expected that a lower mass loss rate may produce a negative spectral index even with a strongly declining synchrotron emissivity. In Fig. 7 we show the cumulative flux for  $\dot{M} = 4.0 \times 10^{-6} M_{\odot} \text{ yr}^{-1}$ , which is a factor 5 lower than the observed  $H\alpha$  mass-loss rate we adopted in the rest of this paper. By restricting the outer boundary of the synchrotron-emitting region to  $430 R_*$ , we find that the model reproduces the observed radio spectrum.

There is no reason to assume, however, that the mass-loss rate of Cyg OB2 No. 9 can simply be lowered by a factor of five. Although the mass-loss rate is extremely high for an O star, Cyg OB2 No. 9 is also extremely bright ( $L_* = 1.74 \times 10^6 L_{\odot}$ ), and it obeys the normal wind-momentum luminosity relation for O stars. It is widely accepted that observed O-star mass-loss rates might be overestimated by a factor of a few due to clumping (e.g. Massa et al. 2003, Hillier et al. 2003). The hydrodynamical simulations on which we have based our model obviously predict a large amount of clumping. However, it is important to realise that a reduced mass-loss rate due to optically thin clumps does not reduce the free-free optical depth if the clumped model is to produce the same thermal flux (see Appendix A). In other words, assuming a clumped wind does not provide a way to reconcile the hydrodynamical predictions

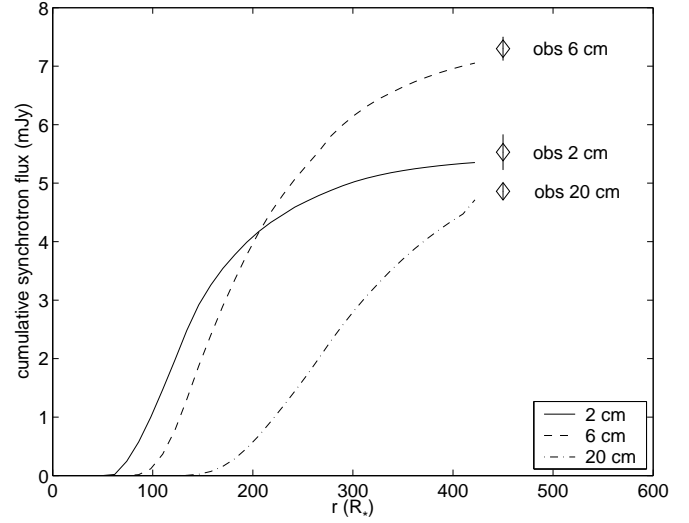


**Fig. 7.** Cumulative fluxes for a synchrotron model with an artificially low mass-loss rate, at 2 cm (solid line), 6 cm (dashed) and 20 cm (dash-dotted). The diamonds are the observed synchrotron fluxes and also the error bar on the observations is given. The model parameters are  $\dot{M} = 4.0 \times 10^{-6} M_{\odot} \text{ yr}^{-1}$ ,  $\Delta u_{\text{max}} = 152 \text{ km s}^{-1}$ ,  $\chi = 3$  and  $B_* = 200 \text{ G}$ . We extrapolated  $\Delta u$  inward, so that, for  $r < 30 R_*$ ,  $\Delta u = 1.74 \Delta u_{\text{max}}$  and, for  $30 R_* < r < 100 R_*$ ,  $\Delta u = 1.39 \Delta u_{\text{max}}$ . A shock is present every  $12 R_*$ .

with the radio observations. Other mechanisms such as porosity (e.g. Owocki et al. 2004), where wind material is packed together also in the lateral direction, may play a rôle when individual clumps become optically thick. Owocki et al. (2004) show that for optically thick clumps the opacity is effectively reduced. Porosity is characterised by an additional parameter (the clump size or equivalent) which complicates the relation between the clump properties and the radio flux. It is as yet unclear to what extent hot-star winds are affected by porosity, if at all.

The O4 main-sequence star 9 Sgr has a much lower mass-loss rate ( $\dot{M} = 2.4 \times 10^{-6} M_{\odot} \text{ yr}^{-1}$ ) than Cyg OB2 No. 9. Therefore, one could expect its spectrum to be compatible with the predicted decline of the shock strength. Figure 8 shows the cumulative flux at 2, 6 and 20 cm for a synchrotron model of 9 Sgr. The adopted parameters are  $T_{\text{eff}} = 43\,000 \text{ K}$ ,  $R_* = 16 R_{\odot}$ ,  $d = 1.58 \text{ kpc}$ ,  $v_{\infty} = 2950 \text{ km s}^{-1}$ ,  $\dot{M} = 2.4 \times 10^{-6} M_{\odot} \text{ yr}^{-1}$ , and  $L_* = 8.1 \times 10^5 L_{\odot}$ . The velocity jump and compression ratio were taken from Fig. 1. The model does not fit the observations, because the theoretical synchrotron spectrum between 6 and 20 cm is essentially flat, contrary to the observed negative spectral index. In this sense the same problems as for Cyg OB2 No. 9 appear, but now at larger wavelengths.

## 5. Conclusions

We have included the radial decline of the shock strength, as predicted by hydrodynamical models, in our synchrotron-emission model for single O stars, and applied it to the widely



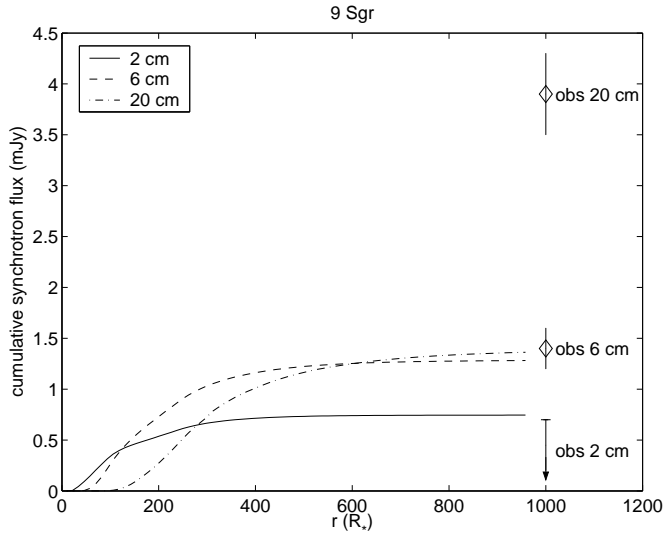


**Fig. 8.** Cumulative fluxes at 2 cm (solid line), 6 cm (dashed) and 20 cm (dash-dotted) for 9 Sgr. The diamonds are the observed synchrotron fluxes and also the error bar on the observations is given. The arrow denotes the upper limit at 2 cm. The model parameters are  $\dot{M} = 2.4 \times 10^{-6} M_{\odot} \text{ yr}^{-1}$ ,  $\Delta u_{\text{max}} = 130 \text{ km s}^{-1}$ ,  $\chi = 3$  and  $B_* = 200 \text{ G}$ . We extrapolated  $\Delta u$  inward in the same way as for Fig. 7. A shock is present every  $12 R_*$ .

presumed single O star Cyg OB2 No. 9, which is a synchrotron emitter. We find that the decline of the shock strength no longer allows a wind-embedded shock model to reproduce the observed negative spectral index of non-thermal emission. We have investigated a number of “escape routes” by which the hydrodynamical predictions might be reconciled with the radio observations. We find that a negative spectral index can be produced by a slower decline of the compression ratio and the velocity jump, by the re-acceleration of electrons in many shocks or by adopting a lower mass-loss rate. However, none of these escape routes are physically very plausible. In particular, re-acceleration by feeding an electron distribution through a number of shocks, is in contradiction with modern hydrodynamical calculations. This leads us to the conclusion that there is probably no viable way to produce the observed spectrum based on hydrodynamical simulations.

Our model obviously has its limitations. Most important, perhaps, is the use of one-dimensional (1D) hydrodynamical simulations. Two-dimensional simulations have been presented for instability-generated structure in the inner wind (Dessart & Owocki 2003). Overall, these models are characterised by a reduced clumpiness of the wind and a larger (radial) velocity dispersion. It is not feasible at present to perform 2D-simulations of the wind out to the distances required for synchrotron-emission models. It cannot be excluded that such models might show a slower decrease of the shock strength. It is to be expected though that as radiative driving becomes negligible at distances of a few tens of stellar radii (Runacres & Owocki 2002), both the compression ratio and the velocity dispersion should eventually decrease even in a 2D model. Furthermore,

2D and 3D hydrodynamics allows for many additional instabilities (such as Rayleigh-Taylor) to disrupt the structure. It is impossible at present to make even an educated guess what a structure of such complexity might mean for the efficiency of synchrotron emission.

Based on the current hydrodynamical simulations, which admittedly are open to question in their details, we suspect that the observed non-thermal radio emission from O stars cannot be explained by wind-embedded shocks associated with the instability of the line-driving mechanism. The most plausible alternative to emission by wind-embedded shocks is emission from shocks associated with colliding stellar winds. That would imply that all non-thermal O stars should be members of a binary or multiple system.

This conclusion is supported by the recent finding (Van Loo 2005, Blomme et al. 2005, Rauw et al. 2005), based on both period analyses of radio light curves and spectroscopic evidence, that three presumably single stars with non-thermal radio emission are probably binaries. Continued systematic radio and spectroscopic monitoring may lead to the same conclusion for the remaining non-thermal radio emitters that are presumed to be single O stars.

*Acknowledgements.* We thank Sean Dougherty, Julian Pittard and Stan Owocki for carefully reading the manuscript and providing valuable comments. We thank the referee, R. L. White, for a constructive report that helped improve the paper. We also thank Achim Feldmeier for useful discussions. SVL gratefully acknowledges a doctoral research grant by the Belgian Federal Science Policy Office (Belspo). Part of this research was carried out in the framework of the project IUAP P5/36 financed by Belspo.

## Appendix A: Effect of clumping on the free-free optical depth

The free-free optical depth is usually calculated assuming a smooth wind (Wright & Barlow 1975) and the effect of density inhomogeneities (clumping) is neglected. However, the line-deshadowing instability packs the stellar wind material together in dense clumps (e.g. Runacres & Owocki 2002). In principle, because the free-free optical depth is proportional to the density squared, one expects clumping to have an influence on the radio photosphere of the stellar wind.

This is indeed the case when we take a given amount of stellar wind material and consider the effect of clumping it. Due to the enhanced opacity of the clumped wind, a given optical depth (integrated from a location in the wind out to the observer) is reached closer to the observer, and as a result the radio photosphere of the stellar wind is larger.

However, if we compare a smooth wind and a clumped wind that produce the same radio flux, the effect of the enhanced optical depth is cancelled exactly by the fact that the clumped wind requires a lower mass loss rate to explain the observations. If we assume a uniform, random distribution of optically thin clumps, then we can use the description of clumping proposed by Abbott et al. (1981). From their Eq. (9) we see that the optical depth has the following dependence on the clumping factor  $f_{\text{cl}}$  and the mass-loss rate

$$\tau_{\nu} \propto \dot{M}^2 f_{\text{cl}}. \quad (\text{A.1})$$

(A succinct explanation of the clumping factor is given in Runacres & Owocki (2002)). The emergent radio flux scales as

$$F_{\nu} \propto (\dot{M}^2 f_{cl})^{2/3} \quad (\text{A.2})$$

(Abbott et al. 1981, their Eq. (10)). Therefore, a clumped wind and a smooth wind that produce the same radio flux will also have the same optical depth. Consequently, a given optical depth is reached at the same radius. This means that, in the limit of optically thin clumps, clumping has no effect on the values we derive for the radio photosphere of the stellar wind.

When individual clumps become optically thick, the Abbott et al. formalism is no longer valid. In that case, porosity effects can play a rôle. Owocki et al. (2004) show that for optically thick blobs the opacity is effectively reduced. Porosity is characterised by an additional parameter (the clump size or equivalent) which complicates the relation between the clump properties and the radio flux.

## References

- Abbott, D. C., Bieging, J. H., & Churchwell, E. B. 1981, *ApJ*, 250, 645
- Bell, A. R. 1978, *MNRAS*, 182, 147
- Benaglia, P., & Koribalski, B. S. 2004, *A&A*, 416, 171
- Benaglia, P., Cappa, C. E., & Koribalski, B. S. 2001, *A&A*, 372, 952
- Bieging, J. H., Abbott, D. C., & Churchwell, E. B. 1989, *ApJ*, 340, 518
- Blomme, R., Van Loo, S., De Becker, M., et al. 2005, *A&A*, 436, 1033
- Bolton, C. T. 1974, *ApJ*, 192, L7
- Chen, W. 1992, Ph.D. Thesis John Hopkins Univ., Baltimore, MD., *Nonthermal radio, X-ray and gamma-ray emissions from chaotic winds of early-type, massive stars*
- Chen, W., & White, R. L. 1994, *Ap&SS*, 221, 259
- De Becker, M., Rauw, G., & Manfroid, J. 2004, *A&A*, 424, L39
- Dessart, L., & Owocki, S. P. 2002, *A&A*, 383, 1113
- Dessart, L., & Owocki, S. P. 2003, *A&A*, 406, L1
- Dougherty, S. M., & Williams, P. M. 2000, *MNRAS*, 319, 1005
- Drake, S. A. 1990, *AJ*, 100, 572
- Drury, L. O'C 1983, *Report Prog. Phys.* 46, 973
- Feldmeier, A. 1995, *A&A*, 299, 523
- Feldmeier, A. 2001, Habilitation thesis Potsdam Univ., *Hydrodynamics of astrophysical winds driven by scattering in spectral lines*
- Garmany, C. D., Conti, P. S., & Massey, P. 1980, *ApJ*, 242, 1063
- Garmany, C. D., & Massey, P. 1981, *PASP*, 93, 500
- Gies, D. R. 1987, *ApJS*, 64, 545
- Gies, D. R., Mason, B. D., Hartkopf, W. I., et al. 1993, *AJ*, 106, 2072
- Harvey, A. S., Stickland, D. J., Howarth, I. D., et al. 1987, *Observatory*, 107, 205
- Hillier, D. J., Lanz, T., Heap, S. R., et al. 2003, *ApJ*, 588, 1039
- Jokipii J. R. 1987, *ApJ*, 313, 842
- Leitherer, C., Forbes, D., Gilmore, A. C., et al. 1987, *A&A*, 185, 121
- Leitherer, C., Chapman, J. M., & Koribalski, B. S. 1995, *ApJ*, 450, 289
- Litvinenko, Y. E. 2003, *Lecture Notes in Physics*, 612, 213
- Lucy, L. B. 1982, *ApJ*, 289, 698
- Massa, D., Fullerton, A. W., Sonneborn, G., Hutchings, J. B. 2003, *ApJ*, 586, 996
- Owocki, S. P. 1991, *IAU Symp.* 143, "Wolf-Rayet Stars and Interrelations with Other Massive Stars in Galaxies", eds. K. A. van der Hucht & B. Hidayat (Kluwer Academic Publishers, Dordrecht), 155
- Owocki, S. P., & Rybicki, G. B. 1984, *ApJ*, 284, 337
- Owocki, S. P., Castor, J. I., & Rybicki, G. B. 1988, *ApJ*, 335, 914
- Owocki, S. P., Gayley, K. G., Shaviv, N. J. 2004, *ApJ*, 616, 525
- Persi, P., Ferrari-Toniolo, M., Tapia, M., et al. 1985, *A&A*, 142, 263
- Rauw, G., Sana, H., Gosset, E., et al. 2005, "Massive Stars and High-Energy Emission in OB Associations", eds. G. Rauw, Y. Nazé, R. Blomme & E. Gosset, 85
- Runacres, M. C., & Owocki, S. P. 2002, *A&A*, 381, 1015
- Runacres, M. C., & Owocki, S. P. 2005, *A&A*, 429, 323
- Setia Gunawan, D. Y. A., De Bruyn, A. G., van der Hucht, K. A., et al. 2003, *ApJS*, 149, 123
- Torres-Dodgen, A. V., Tapia, M., & Carroll, M. 1991, *MNRAS*, 249, 1
- Van Loo, S. 2005, Ph.D. thesis K. U. Leuven, *Non-thermal radio emission from single hot stars*, URL: <http://hdl.handle.net/1979/53>
- Van Loo, S., Runacres, M.C., & Blomme, R. 2004, *A&A*, 418, 717 (Paper I)
- Van Loo, S., Runacres, M.C., & Blomme, R. 2005, *A&A*, 433, 313 (Paper II)
- Walborn, N. R. 2002, in "A Massive Star Odyssey: from Main Sequence to Supernova", eds. K. A. van der Hucht, A. Herrero, & C. Esteban, *ASP Conf. Ser.* 212, 13
- Weber, E. J., & Davis, L. Jr. 1967, *ApJ*, 148, 217
- White, R. L. 1985, *ApJ*, 289, 698
- White, R. L., & Chen, W. 1994, *Ap&SS*, 221, 295
- Wright, A. E., & Barlow, M. J. 1975, *MNRAS*, 170, 41

## List of Objects

- 'Cyg OB2 No. 9' on page 1
- 'HD 93129A' on page 2
- 'HD 93250' on page 2
- '9 Sgr' on page 2
- 'CD-47°4551' on page 2
- 'Cyg OB2 No. 9' on page 2
- 'HD 150136' on page 2
- 'HD 168112' on page 2
- 'HD 15558' on page 2
- 'Cyg OB2 No. 8A' on page 2
- 'Cyg OB2 No. 5' on page 2
- 'HD 124314' on page 2
- 'Cyg OB2-335' on page 2
- '15 Mon' on page 2
- 'HD 167971' on page 2
- 'δ Ori A' on page 2
- 'σ Ori AB' on page 2
- 'Cyg OB2 No. 9' on page 2
- 'Cyg OB2 No. 9' on page 3
- 'Cyg OB2 No. 9' on page 4
- 'Cyg OB2 No. 9' on page 4
- 'Cyg OB2 No. 9' on page 7
- '9 Sgr' on page 7
- 'Cyg OB2 No. 9' on page 7
- 'Cyg OB2 No. 9' on page 8
- 'Cyg OB2 No. 9' on page 8
- '9 Sgr' on page 8

'Cyg OB2 No. 9' on page 8

'9 Sgr' on page 8

'Cyg OB2 No. 9' on page 8

'9 Sgr' on page 9

'Cyg OB2 No. 9' on page 9